

## RESEARCH ARTICLE

10.1029/2018JD028414

## Special Section:

Water-soil-air-plant-human nexus: Modeling and observing complex land-surface systems at river basin scale

## Key Points:

- The AFA method is used to analyze soil moisture persistence
- The persistence and corresponding time scales of soil moisture can be described using a three-phase concept diagram
- Soil moisture persistence is influenced by net radiation and precipitation differently over these three phases

## Supporting Information:

- Supporting Information S1

## Correspondence to:

C. Cheng and C. Song,  
chengcx@bnu.edu.cn;  
songcq@bnu.edu.cn

## Citation:

Shen, S., Ye, S., Cheng, C., Song, C., Gao, J., Yang, J., et al. (2018). Persistence and corresponding time scales of soil moisture dynamics during summer in the Babao River Basin, Northwest China. *Journal of Geophysical Research: Atmospheres*, 123, 8936–8948. <https://doi.org/10.1029/2018JD028414>





Received 31 JAN 2018

Accepted 13 JUL 2018

Accepted article online 28 JUL 2018

Published online 2 SEP 2018

## Persistence and Corresponding Time Scales of Soil Moisture Dynamics During Summer in the Babao River Basin, Northwest China

Shi shen<sup>1,2,3</sup> , Sijing Ye<sup>1,3</sup>, Changxiu Cheng<sup>1,2,3</sup> , Changqing Song<sup>1,3</sup> , Jianbo Gao<sup>4</sup>, Jing Yang<sup>1,2,3</sup>, Lixin Ning<sup>1,2,3</sup> , Kai Su<sup>1,2,3</sup>, and Ting Zhang<sup>1,2,3</sup>

<sup>1</sup>State Key Laboratory of Earth Surface Processes and Resource Ecology, Beijing Normal University, Beijing, China, <sup>2</sup>Key Laboratory of Environmental Change and Natural Disaster, Beijing Normal University, Beijing, China, <sup>3</sup>Center for Geodata and Analysis, Faculty of Geographical Science, Beijing Normal University, Beijing, China, <sup>4</sup>Institute of Complexity Science and Big Data Technology, Guangxi University, Nanning, China

**Abstract** Soil moisture (SM) is an essential Earth surface and climate system variable. Insights into its persistence and corresponding time scales can improve numerical modeling and climate system prediction. In this study, SM from 17 observation stations within the Babao River Basin, Northwest China, between 1 June and 31 August 2014 were used to investigate persistence and corresponding time scales via adaptive fractal analysis. By conducting an adaptive fractal analysis of net radiation and by estimating the complementary cumulative distribution function of precipitation intervals, the relation between meteorological factors and the persistence and time scales of SM are determined and discussed. Results show that persistence and corresponding time scales of SM could be described using a three-phase concept diagram. (1) At short time scales (approximately 0–14 hr [4 cm], 0–15 hr [10 cm], or 0–19 hr [20 cm]), the persistence of SM at most observation stations shows a strong long-range correlation or nonstationarity. This phenomenon is essentially due to evaporation influenced by net radiation processes and the effects of rain. (2) At moderate time scales (approximately 14–159 hr [4 cm], 15–161 hr [10 cm], or 19–143 hr [20 cm]), the persistence of SM mostly exhibits a weak long-range correlation or antipersistence due to net radiation process uncertainty and the probability of precipitation. (3) At long time scales (approximately greater than 159 hr [4 cm], 161 hr [10 cm], and 143 hr [20 cm]), the persistence of SM dynamics exhibits antipersistence because a high probability of precipitation reverses changes in the SM persistence.

### 1. Introduction

Soil moisture is a critical factor that affects numerous Earth surface processes, as well as physical and chemical feedback cycles. Soil moisture significantly affects land-atmosphere interactions by changing water and energy balance (Koster & Suarez, 2003; Seneviratne et al., 2010). Additionally, soil moisture status is related to runoff (Brocca et al., 2010; Koster et al., 2010), heat waves (Hirschi et al., 2010), air temperature (Janatian et al., 2017), and precipitation patterns (Mei & Wang, 2011; Tuttle & Salvucci, 2016). In the field of geophysics, much of the research on soil moisture has focused on characteristics of soil moisture such as spatiotemporal patterns and variability (Gebremichael et al., 2009; Brocca et al., 2012; Vereecken et al., 2014) and on the relationship between impact factors (e.g., soil type, land cover, precipitation, insolation, air temperature, and ground temperature) and soil moisture (Bosch et al., 2006; Cho & Choi, 2014; Famiglietti et al., 1999; Sun & Wang, 2012). In addition, many studies have discussed spatial scaling effects and spatial scaling invariance properties observed with typical fractal geometric features such as fractal dimensions (Ji et al., 2016; Millán et al., 2016; Vidal-Vazquez et al., 2012).

While considerable research has been conducted on spatial scaling effects and spatial scaling invariance properties, the persistence and corresponding time scale of soil moisture dynamics observed over time have been insufficiently studied from a fractal perspective. Unlike other definitions (Ghannam et al., 2016), the definition of soil moisture persistence used in this study refers to its long-range correlation (known as long-range dependence, long memory, or long-range persistence) and antipersistence. Whether soil moisture exhibits a long-range correlation or antipersistence, corresponding time window sizes are defined as corresponding time scales. Fractal or multifractal behaviors have often been studied to describe soil moisture dynamics

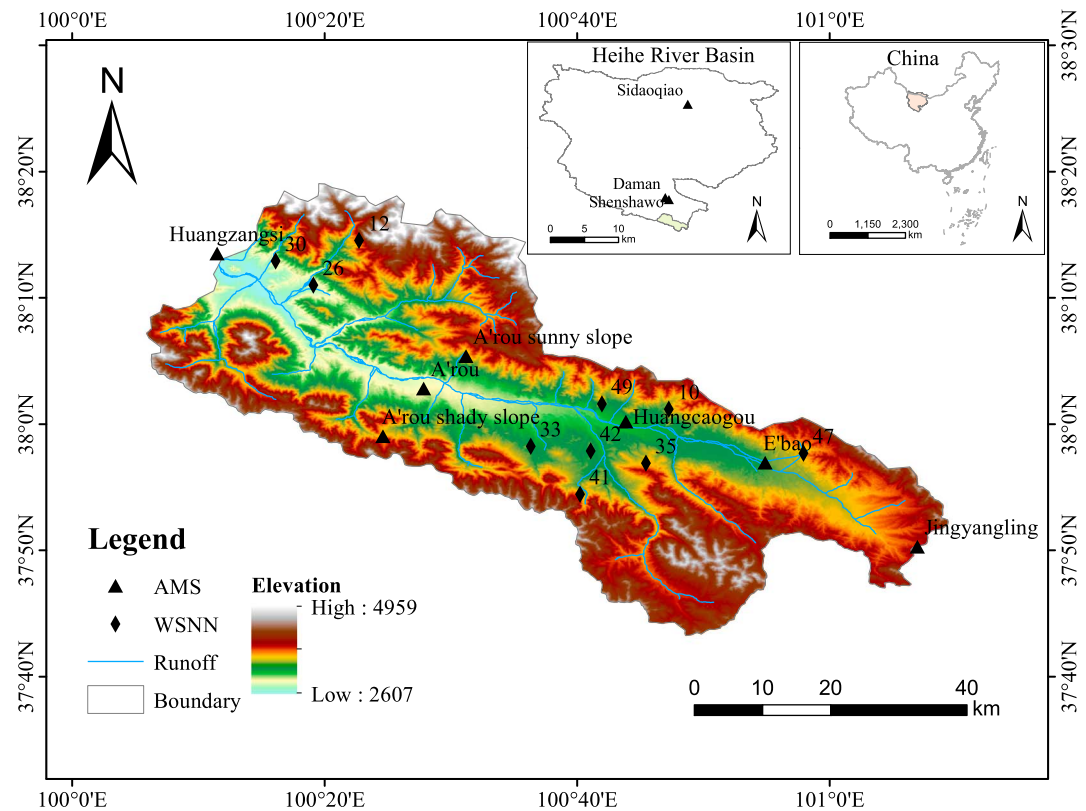


**Figure 1.** A map of the Babao River Basin, Northwest China showing the study area, automatic monitoring stations (AMSs), and wireless sensor network nodes (WSNNs).

(Gao et al., 2015; Guerrini & Swartzendruber, 1997; Mirás-Avalos et al., 2016). Various studies (e.g., R. Song et al., 2011; Gao et al., 2015; Ji et al., 2016; Mirás-Avalos et al., 2016) have focused on the features (e.g., fractal dimensions and long-range correlations) of soil moisture dynamics. Various studies demonstrate that soil moisture dynamics present significant long-range correlations in different areas (Gao et al., 2015; R. Song et al., 2011). Orth and Seneviratne (2012) analyzed seasonal variation and climatic factors of soil moisture persistence in Europe. However, relationships between external factors (e.g., precipitation and insolation) and the persistence and corresponding scales of soil moisture dynamics must still be examined.

It is also necessary to enhance the description, investigation, and understanding of soil moisture persistence and of corresponding time scale to improve the accuracies of soil moisture simulations using linear models or models considering nonlinearity, as soil moisture is clearly nonlinear and complex over time when coupled with environmental factors and processes (Mirás-Avalos et al., 2016). First, the soil water diffusivity, which is illustrated by fractional Brownian motion, follows a nonrandom, nonstationary process and fractal behavior (Guerrini & Swartzendruber, 1997). Second, the meteorological and hydrological processes are nonlinear and persistent (Bunde & Havlin, 2002; Bunde et al., 2001; Z. Liu et al., 2017; Schertzer et al., 2010; Zhao et al., 2017). Finally, integrated and conjunct effect of external factors (i.e., precipitation and insolation) on soil moisture dynamics are also nonlinear. Generated soil moisture simulation data should exhibit the soil moisture persistence at different time scales under various precipitation/net radiation conditions. From this perspective, the persistence plays a referential role in improving the accuracy of soil moisture simulations.

Another goal of ours was to examine the relationship between soil moisture dynamic persistence and precipitation, persistence, and net radiation. While the meteorological factors (e.g., evapotranspiration, precipitation, and insolation) can directly or indirectly change soil moisture (Bosch et al., 2006; Cho & Choi, 2014; Famiglietti et al., 1999), the relationship between the persistence and corresponding time scales of soil moisture dynamics and meteorological factors remains unclear. At different time scales the main meteorological factors that influence soil moisture vary. Time scales and the corresponding main factor will testify to the model accuracy and provide useful information for the management of irrigation and for monitoring drought. We focus

**Table 1**  
*AMSs and WSNNs Spatial Information*

ID	Name/code	Station type	Sensor type	Latitude (°N)	Longitude (°E)	Elevation (m)
1	A'rou	AMS	Hydra Probe II	38.047	100.464	3,033
2	A'rou sunny slope	AMS	Hydra Probe II	38.090	100.520	3,529
3	A'rou shady slope	AMS	Hydra Probe II	37.984	100.411	3,536
4	Huangzangsi	AMS	Hydra Probe II	38.225	100.192	3,294
5	Huangcaogou	AMS	Hydra Probe II	38.003	100.731	3,137
6	Jingyangling	AMS	Hydra Probe II	37.838	101.116	3,750
7	E'Bao	AMS	Hydra Probe II	37.949	100.915	3,294
8	10	WSNN	SISOMOP	38.020	100.788	3,484
9	12	WSNN	SISOMOP	38.243	100.379	3,766
10	26	WSNN	SISOMOP	38.184	100.319	3,045
11	30	WSNN	SISOMOP	38.216	100.269	3,091
12	33	WSNN	SISOMOP	37.971	100.606	3,335
13	35	WSNN	SISOMOP	37.949	100.758	3,335
14	41	WSNN	SISOMOP	37.908	100.671	3,635
15	42	WSNN	SISOMOP	37.965	100.685	3,413
16	47	WSNN	SISOMOP	37.962	100.966	3,515
17	49	WSNN	SISOMOP	38.027	100.700	3,661
18	Daman	AMS	Hydra Probe II	38.856	100.372	1,556
19	Shenshawo	AMS	Hydra Probe II	38.789	100.493	1,594
20	Sidaoqiao	AMS	Hydra Probe II	42.001	100.137	873

*Note.* AMS = automatic monitoring station; WSNN = wireless sensor network node; SISOMOP = simplified soil moisture probe.

on the relationship between corresponding time scales for persistence and the time intervals of precipitation and between corresponding time scales for persistence and net radiation time scales. While an adaptive fractal analysis (AFA) of soil moisture for the Babao River Basin (BRB) was carried in this study, the method can be applied to other basins as well.

The BRB is selected as a study area reflective of arid and semiarid regions. Due to its mountainous terrain, the BRB serves as an important headwater area for this arid region (Tian et al., 2017). On the one hand, the soil moisture directly reflects soil water content and significantly affects runoff and soil erosion patterns (Fitzjohn et al., 1998). On the other hand, the ways in which soil moisture dynamics change over different time scales are essential to examine in managing the ecosystem, land use, and water resources (Daly & Porporato, 2005). Therefore, understanding soil moisture dynamics in arid regions (e.g., the BRB) is vital to local land use management, water resource regulation, and ecosystem protection (Kurc & Small, 2007; C. Song et al., 2017).

In the present study, the Hurst exponent was used to denote the persistence of soil moisture dynamics. In addition, linear scaling ranges are identified and analyzed as they are essential to scaling and fractal analyses in practice (Gao et al., 2006). The remainder of this paper is organized as follows. Section 2 introduces the study area, data sources, and methodology used. The results for the AFA of soil moisture and on the relation between meteorological factors and soil moisture dynamics are given in section 3. A brief discussion of soil moisture dynamics is presented in section 4. Section 5 presents the conclusions of this study and planned future work.

## 2. Method and Data Sources

### 2.1. Study Area

The study area and locations of the 17 observation stations used in this study are shown in Figure 1. The BRB covers an area of 2,450 km<sup>2</sup> (Ge et al., 2015) in the upper reaches of the Heihe River Basin, the second largest inland basin in China. This region is a typical arid and high-latitude mountainous region. The annual precipitation for the region is measured at approximately 405 mm/year with most rainfall occurring during the summer (from June to August). The mean annual temperature for the region is approximately 0.4 °C (Luo et al.,

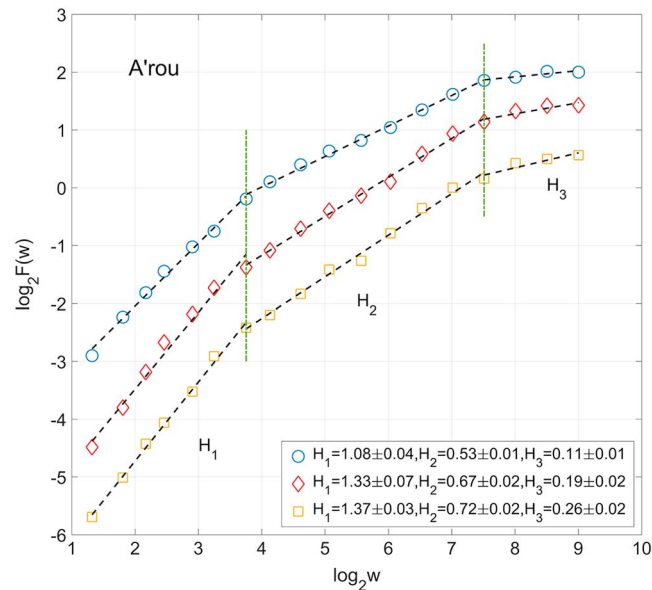


**Figure 2.** Adaptive fractal analysis of soil moisture for 1 June to 31 August 2014 for depths of 4 (blue circles), 10 (red diamonds), and 20 cm (yellow squares) for the A'rou automatic monitoring station. Black dashed lines show the linear fitting of  $\log_2 F(w)$  and  $\log_2 w$  of each scaling ranges, which are separated by green vertical lines.  $H_1$ ,  $H_2$ , and  $H_3$  represent Hurst exponents of soil moisture measured at short, moderate, and long time scales, respectively. Interval estimations represent the standard errors for linear least squares fitting.

2017). The main soil type is Matti-Gelic Cambosols (China Soil Taxonomy). The local land cover type include alpine meadows, grassland, shrubland, sparse vegetation, and forest. Moreover, three automatic monitoring stations (AMSs) outside of the BRB region, Daman, Shenshawo, and Sidaoqiao, which are located in the middle and lower reaches of the Heihe River Basin, are also studied for comparison.

## 2.2. Data

Soil moisture, precipitation, and net radiation data for 1 June to 31 August 2014 were provided by Environmental and Ecological Science Data Center for West China, National Natural Science Foundation of China (Li et al., 2013; S. Liu et al., 2011). Soil moisture in situ data drawn from three depths (4, 10, and 20 cm) were received from 10 AMSs and from 10 wireless sensor network nodes. Both the precipitation and net radiation data were obtained from the 10 AMSs. The detailed information of AMSs and wireless sensor nodes are listed in Table 1. In addition, all of the data used were resampled as hourly average data to unify the sampling frequency.

## 2.3. Adaptive Fractal Analysis

Since the long-range correlation was first presented by Hurst, numerous methods have been developed (e.g., the rescaled range analysis, detrended fluctuation analysis, and AFA; Gao et al., 2007; Hurst, 1951; Peng et al., 1994). However, AFA presents advantages over rescaled range analysis and detrended fluctuation analysis in managing arbitrary and strong nonlinear trends (Gao et al., 2011; Hu et al., 2009) due to the finer resolution of fractal scaling behavior considered within short time series (Gao et al., 2012) and due to its more accurate Hurst exponent estimations (Gao et al., 2011). Therefore, AFA has been widely used to analyze the persistence and severity of global terrorism trends (Gao et al., 2017), sociocultural phenomena (Gao et al., 2012), electricity power load (Jiang & Gao, 2016), traffic flow (Zhu & Gao, 2014), and bioinformatics patterns (Gao et al., 2011; Gao et al., 2013; Sengupta et al., 2017).

A soil moisture time series can be regarded as involving fractional Brownian motion and is denoted as an  $1/f^{2H+1}$  process, where  $f$  denotes the frequency and  $H$  is the Hurst exponent (Gao et al., 2006). This type of process presents long-range correlations when  $0.5 < H < 1$ , short-range correlations when  $H = 0.5$ , and antipersistent correlations when  $0 < H < 0.5$  (Gao et al., 2007). Moreover, the Hurst exponent can be larger than 1, showing that the process is nonstationary rather than stationary (Gao et al., 2006; Gao et al., 2012).

A typical AFA procedure can be described as follows. First, global trends  $v(i)$  of a random walk process  $u(i)$ ,  $i = 1, 2, \dots, N$  are identified, where  $N$  is the length of the original data. Global trends are identified from synthesized local polynomial fitting trends of  $n+1$  original data points found in overlapped windows of length

**Table 2**  
Hurst Exponents of Soil Moisture for Depths of 4, 10, and 20 cm for 17 In Situ Observation Stations

Name/code	4 cm			10 cm			20 cm		
	$H_1$	$H_2$	$H_3$	$H_1$	$H_2$	$H_3$	$H_1$	$H_2$	$H_3$
A'rou	1.08	0.53	0.11	1.33	0.66	0.18	1.37	0.72	0.26
A'rou sunny slope	1.12	0.49	0.09	1.06	0.56	0.19	1.23	0.63	0.18
A'rou shady slope	1.14	0.54	0.21	1.09	0.48	0.18	1.01	0.49	0.17
Huangzangsi	0.74	0.42	0.12	0.80	0.42	0.10	0.74	0.29	0.06
Huangcaogou	1.14	0.61	0.15	1.24	0.62	0.12	1.00	0.58	0.13
Jingyangling	0.97	0.76	0.39	0.96	0.76	0.39	1.25	0.81	0.48
E'bao	0.83	0.42	0.07	0.88	0.48	0.12	1.23	0.59	0.19
10	0.73	0.38	0.10	1.01	0.52	0.10	0.93	0.59	0.12
12	0.79	0.48	0.14	0.91	0.59	0.26	0.7	0.7	0.22
26	0.89	0.46	0.15	0.92	0.54	0.23	0.89	0.51	0.25
30	0.95	0.52	0.17	1.04	0.63	0.22	0.85	0.52	0.22
33	1.12	0.61	0.19	1.19	0.56	0.18	0.66	0.52	0.19
35	0.55	0.55	0.19	0.86	0.36	0.36	0.65	0.36	0.16
41	0.95	0.35	0.18	0.99	0.37	0.19	0.79	0.52	0.06
42	0.96	0.54	0.18	1.10	0.55	0.19	0.70	0.70	0.25
47	0.69	0.48	0.15	0.77	0.49	0.12	0.58	0.58	0.17
49	1.08	0.53	0.08	1.06	0.53	0.07	0.79	0.53	0.08
Daman	0.81	0.47	0.15	0.86	0.48	0.20	0.90	0.56	0.42
Shenshawo	0.99	0.49	0.07	1.25	0.58	0.16	1.43	0.59	0.22
Sidaoqiao	1.76	0.04	0.04	1.77	0.05	0.05	1.78	0.15	0.15

$w = 2n + 1$ , where  $n$  is a chosen parameter. In addition, the polynomial model for fitting local trend typically uses a linear or quadratic function. As a result, detrended data  $y(i)$  (i.e., the residual of original data to global trend) are as follows:

$$y(i) = u(i) - v(i). \tag{1}$$

Subsequently, the relationship between the variance of the magnitude of residuals  $F(w)$  and the length of the window  $w$  is then examined.

$$F(w) = \left[ \frac{1}{N} \sum_{i=1}^N (u(i) - v(i))^2 \right]^{1/2} \sim w^H. \tag{2}$$

Using the ordinary least squares estimation for double logarithmic coordinates, the Hurst exponent  $H$  and linear scaling ranges can be identified through slopes and ranges of linear fitting, respectively.

### 3. Results and Analysis

#### 3.1. Persistence of In Situ Soil Moisture

An AFA of hourly soil moisture was conducted for each monitoring site (see supporting information Figures S1–S17 for detailed results). Taking the A'rou station as an example, Figure 2 shows the resultant AFA of soil moisture for three depths for the A'rou station. As is shown in Figure 2,  $\log_2 F(w)$  and  $\log_2(w)$  represent the binary logarithm of the residuals magnitude variance and the length of the window, respectively. Blue circles, red diamonds, and yellow squares denote the soil moisture observed at 4, 10, and 20 cm, respectively. Black dashed lines denote the linear fitting of  $\log_2 F(w)$  and  $\log_2(w)$  for each of the scaling ranges, which are separated by green vertical dashed lines.  $H_1$ ,  $H_2$ , and  $H_3$  denote the Hurst exponents of soil moisture for short, moderate, and long time scale ranges, respectively.

Several features are identified from Figures 2 and S1–S17 and Table 2. First, the multisegment scaling ranges, which indicate the range of time scales corresponding to Hurst exponents  $H_1$ ,  $H_2$ , and  $H_3$ , are clearly identifiable because  $\log_2 F(w)$  and  $\log_2(w)$  present linear relationship within each scaling range.

**Table 3**  
Linear Scaling Range Estimators of Soil Moisture for Depths of 4, 10, and 20 cm

Name/code	4 cm		10 cm		20 cm	
	E1	E2	E1	E2	E1	E2
A'rou	3.75	7.51	3.75	7.51	3.75	7.51
A'rou sunny slope	3.75	7.02	3.75	7.02	3.75	7.02
A'rou shady slope	4.13	7.51	4.13	7.51	4.13	7.51
Huangzangsi	3.75	7.51	3.75	7.51	3.75	7.51
Huangcaogou	3.25	7.51	3.25	7.51	3.26	7.51
Jingyangling	4.13	5.07	4.13	5.07	4.13	5.07
E'bao	3.75	7.51	3.75	7.51	3.75	7.51
10	4.13	7.51	4.13	7.51	4.13	7.51
12	4.13	7.51	4.13	7.51	/	7.51
26	3.25	7.51	4.61	7.51	5.07	7.51
30	4.13	7.51	4.13	7.51	5.07	7.51
33	3.75	7.51	3.75	7.51	5.07	7.51
35	/	7.02	4.61	/	5.07	7.51
41	3.75	7.51	3.75	7.51	3.75	4.51
42	4.13	7.51	4.13	7.51	/	7.51
47	4.13	7.51	4.13	7.51	/	7.51
49	3.75	7.51	3.75	7.51	5.07	7.51
Daman	3.75	7.51	3.75	7.51	5.07	7.51
Shenshawo	3.75	7.51	3.75	7.51	5.07	7.51
Sidaoqiao	3.75	7.51	3.75	7.51	5.07	7.51

Note. A slash indicates that there are none of this type of estimator.

In addition, when only two scaling ranges are considered,  $H_2$  is considered equal to the corresponding  $H_1$  or  $H_3$  depending on where the break is positioned to maintain the consistency of descriptions. Second, three Hurst exponents of the same depth successively decrease for the same observation station. With the exception of those for the wireless sensor network node (WSNN) #35 station, AFA curves are shown from top to bottom for three depths (4, 10, and 20 cm). Third,  $H_1$  values are generally larger than 0.5 and are sometimes even larger than 1, indicating the nonstationarity of soil moisture. In turn, soil moisture will continue to significantly increase or decrease over short time periods.  $H_2$  fluctuates by approximately 0.5 but does not exceed  $H_1$ . Therefore, soil moisture will have a high probability of continuing to increase or decrease within a moderate time scale.  $H_3$  is slightly lower than both 0.5 and the corresponding  $H_2$ . Similarly,  $H_3$  of long time scales shows that soil moisture is likely to shift from decreasing to increasing or from increasing to decreasing. Finally, soil moisture was found to present one or two scaling region breaks, revealing turning points of the Hurst exponents. These turning points show that soil moisture trends reverse from a moderate time scale to large time scale.

In addition, estimators of linear scaling ranges for our AFA of soil moisture time series are shown in Table 3. The two estimators indicate the break points of time scales for different time scaling ranges.  $E1$  and  $E2$  are obtained from the corresponding value of  $\log_2(w)$  for each break point.  $E1$  indicates the maximum time scale of short time scale ranges and the minimum time scale of the moderate time scaling range.  $E2$  indicates the maximum time scale of the moderate time scaling range and the minimum time scale of the long time scale range.

In general, most of the scaling ranges present two estimators  $E1$  and  $E2$ , denoting the time scale of  $2^{E1}$  and  $2^{E2}$  hr, respectively. According to the Hurst exponents and scaling ranges of 17 stations in the BRB, the persistence of soil moisture dynamics can be divided into three phases. (1) Phase

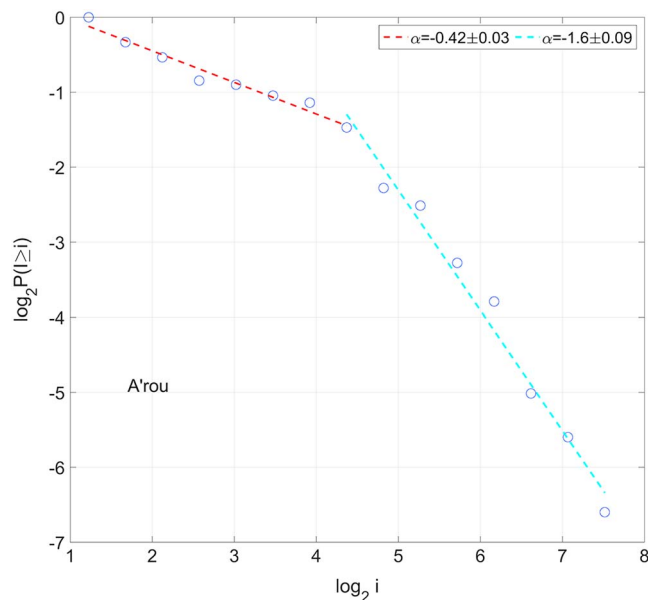


**Figure 3.** CCDF of intervals between continuous hourly precipitation for the A'rou station in log-log form.  $\log_2 i$  and  $\log_2 P(l > i)$  represent logarithms to base 2 of the intervals and corresponding CCDF values. Dashed red and cyan lines denote the best linear fitting found for the scaling ranges. The  $\alpha$  is the slope of the linear least squares fitting. CCDF = complementary cumulative distribution function.

**Table 4**  
Linear Scaling Range Estimators of Precipitation CCDF for Seven AMSs of the BRB Region

Name	Scaling break	Tail estimator
A'rou	4.371	7.517
A'rou sunny slope	4.365	8.506
A'rou shady slope	4.430	6.850
Huangzangsi	4.336	7.450
Huangcaogou	5.126	6.698
Jingyangling	4.129	6.355
E'bao	4.266	7.314

Note. CCDF = complementary cumulative distribution function; AMSs = automatic monitoring stations; BRB = Babao River Basin.

1: For the short time scale (approximately 0–14 hr at 4 cm, 0–15 hr at 10 cm, and 0–19 hr at 20 cm on average), the persistence of soil moisture dynamics exhibits a strong pattern of nonstationarity or long-range correlation. (2) Phase 2: For the moderate time scale (approximately 14–159 hr at 4 cm, 15–161 hr at 10 cm, and 19–143 hr at 20 cm on average), the persistence of soil moisture dynamics shows a weak long-range correlation or antipersistence. (3) Phase 3: For the long time scale (approximately more than 159 hr at 4 cm, more than 161 hr at 10 cm, and more than 143 hr at 20 cm on average), the persistence of soil moisture dynamics presents a strong antipersistence trend. The stations present two scaling ranges that conclude within two of the three phases, though exact time scales differ based on the two phases involved. For example, soil moisture dynamics observed at 4 cm for Huangcaogou station involved Phases 1, 2, and 3 for time scales of 9.5, 9.5–182, and longer than 183 hr, respectively. Accurate time scales for each phase vary from one station to another because the geographic factors (e.g., slope, aspect, elevation, and vegetation coverage) affecting the stations are not identical.

The Hurst exponents and scaling ranges can enhance our understanding of the soil system and can help improve models and agricultural planning. In terms of improving models, the persistence and time scales can be used to identify the proper time scale for downscaling soil moisture remote sensing data. Regarding the agricultural planning, the resultant persistence and corresponding time scale presented in this paper can be used to determine how soil moisture conditions will develop in the future. For example, when soil moisture levels in an area reflect arid conditions, we can determine whether droughts or high wetting levels are likely to occur according to the Hurst exponent and its time scale.

### 3.2. Relationships Between Scaling Range Estimators of Soil Moisture and Precipitation

As precipitation occurs at intervals and directly changes the soil moisture conditions, a scatter plot of soil moisture scaling ranges and scaling breaks of precipitation intervals is used to verify whether there is a relationship between them.

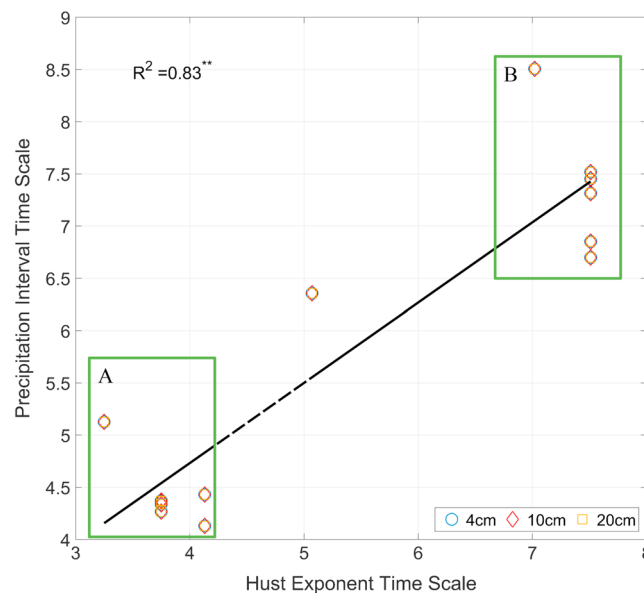


**Figure 4.** Relationships between Hurst exponent time scaling range estimators for soil moisture and time scaling estimators for precipitation intervals. The horizontal axis denotes scaling range estimators of the Hurst exponent. The vertical axis denotes the scaling break and tail estimator (i.e., scaling range estimators) of the CCDF of precipitation intervals. Circles, diamonds, and squares denote scaling ranges of the Hurst exponent and the CCDF of precipitation intervals for depths of 4, 10, and 20 cm for seven automatic monitoring stations in the Babao River Basin. CCDF = complementary cumulative distribution function.

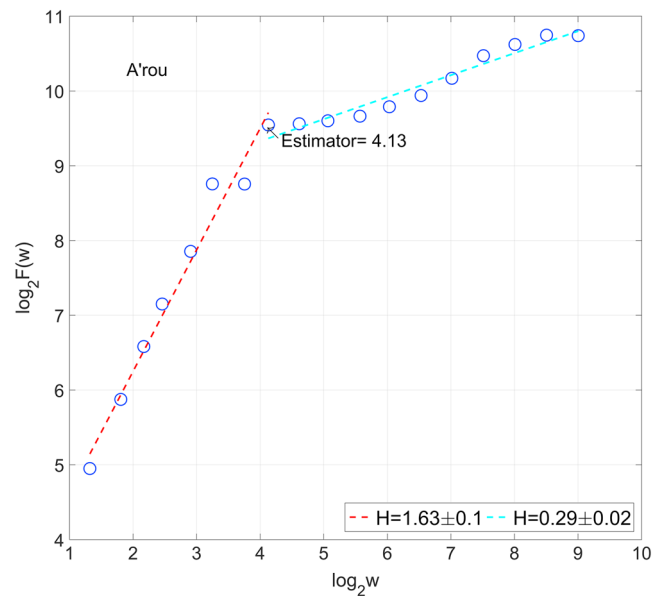


**Figure 5.** Adaptive fractal analysis of net radiation for 1 June to 31 August 2014, for the A'rou automatic monitoring stations. Dashed lines denote the linear fitting of  $\log_2 F(w)$  and  $\log_2 w$  for each of the scaling ranges, which are separated at the estimator.

The complementary cumulative distribution function (CCDF) of intervals of continuous hourly precipitation was calculated using a log-log plot to determine scaling region breaks. As the 10 WSNNs lost considerable amount of precipitation data and are not equipped with radiation sensors, only precipitation and net radiation data for 10 AMSs were used. For example, the precipitation CCDF for the A'rou station is shown in Figure 3 where  $\log_2 i$  and  $\log_2 P(i > i)$  represent logarithms to base 2 of the intervals and corresponding CCDF values. The dashed red and cyan lines denote the best linear fittings found for the scaling ranges. The  $\alpha$  is the slope of the linear least squares fitting. Some features are identified from Figures 3 and S21–S30. The CCDF curves of precipitation intervals reveal a power law generated from two well-distinguished linear fitting sections in log-log coordinates. The  $\alpha$  significantly decreases following scaling breaks. To distinctly illustrate the scaling breaks and the tail estimator of the intervals, CCDF parameters for seven AMSs of the BRB region are listed in Table 4. The tails of interval logarithms drop from approximately 6.3 to 7.5.

The  $E1$  and  $E2$  of soil moisture scaling ranges correspond to the scaling break and tail estimator of precipitation intervals, respectively. This is defined naturally because  $E1$  and  $E2$  refer to short and long time scales, respectively. At the same time, the scaling break and tail breaks represent short and long time intervals, respectively. The resulting scatter diagram is shown in Figure 4 where circles, diamonds, and squares denote scaling breaks for depths of 4, 10, and 20 cm, respectively. The Hurst scale represents Hurst exponent scaling ranges of soil moisture. Interval scales represent the scaling breaks and tail estimators of precipitation intervals.

There is a well-fitted linear relationship between the Hurst exponent time scale and precipitation interval scales. The coefficient of determination  $R^2$  is equal to 0.88, which is significant at the 0.01 level. The Hurst exponent time scale represents ranges of long-range correlation or antipersistence. Additionally, the interval scale identifies regions of low or high rainfall probability. As is shown in Figure 4, the scatters in region A demonstrate time scales presenting low precipitation probability and long-range soil moisture correlations (or nonstationarity). The scatters shown in region B demonstrate time scales with high precipitation probability and soil moisture antipersistence. Although the scatters are mostly located in regions A and B, relationships are still relatively reasonable given that scaling range estimators of soil moisture observed at three depths and scaling range estimators of precipitation intervals show similar trends. Therefore, the influence of precipitation on soil moisture can be characterized by the scaling ranges of Hurst exponents and by precipitation intervals. According to these results, soil moisture simulation can be improved by modifying the weight of net radiation and precipitation effects on soil moisture at different time scales.



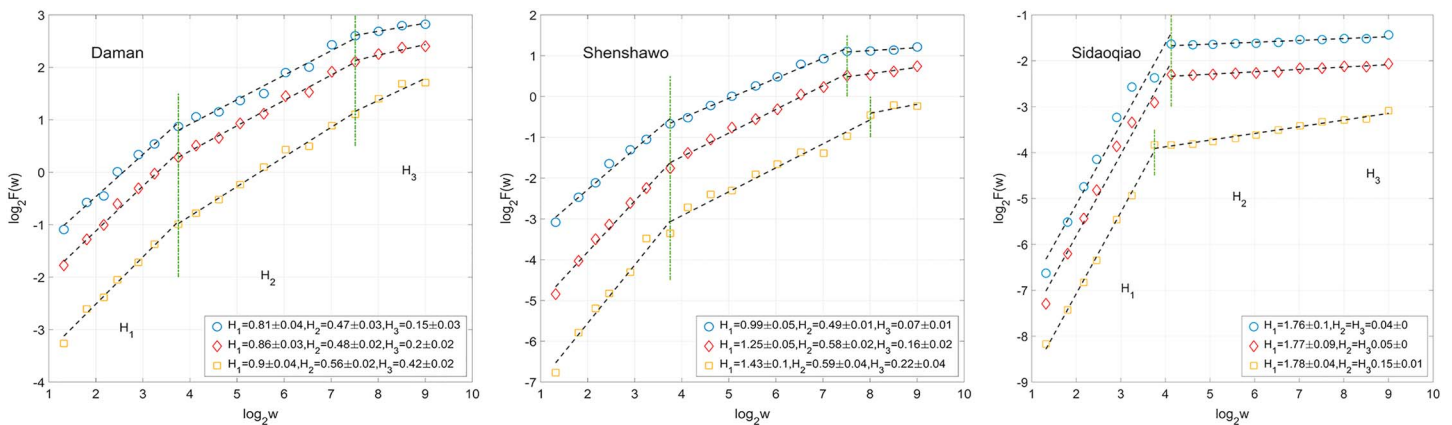


**Figure 6.** Adaptive fractal analysis of soil moisture for 1 June to 31 August 2014 for the depths of 4 (blue circles), 10 (red diamonds), and 20 cm (yellow squares) for Daman, Shenshawo, and Sidaoqiao automatic monitoring stations. Dashed black lines denote linear fitting of  $\log_2 F(w)$  and  $\log_2 w$  values for each scaling ranges, which are separated by green vertical lines.

### 3.3. Scaling Range Estimators of Net Radiation

In addition to precipitation, solar radiation affects soil moisture dynamics, as it significantly affects evapotranspiration from the land surface and especially over short periods of time. The hourly average net radiation value is used to represent the solar radiation effect on the soil moisture system, as net radiation removes other influences (e.g., shortwave and atmospheric radiation). An AFA of net radiation for 10 AMSs is performed (see Figures S31–S40). Figure 5 shows the AFA of net radiation for 1 June to 31 August 2014 for A'rou AMSs. Dashed lines denote the linear fitting for all of the scaling ranges separated at the estimator. Net radiation exhibits significant nonstationarity over a short time scale. Therefore, net radiation processes present distinct nonstationary dynamics over short time scales, echoing the short scales of soil moisture dynamics.

### 3.4. Comparison of Stations Characterized by Different Vegetation Types

Since the vegetation type of the 17 stations in the BRB is the alpine meadow, in order to evaluate water uptakes by local vegetation, three more stations located in the middle reach (Shenshawo and Daman) and lower reach (Sidaoqiao) of the Heihe River Basin are also analyzed. The land cover at the Shenshawo station is characterized by features of the Gobi Desert. Land cover at Daman station is mainly composed of maize farmland. Chinese Tamarisk vegetation is the main type of vegetation found in the Sidaoqiao station. Figure 6 shows AFA results

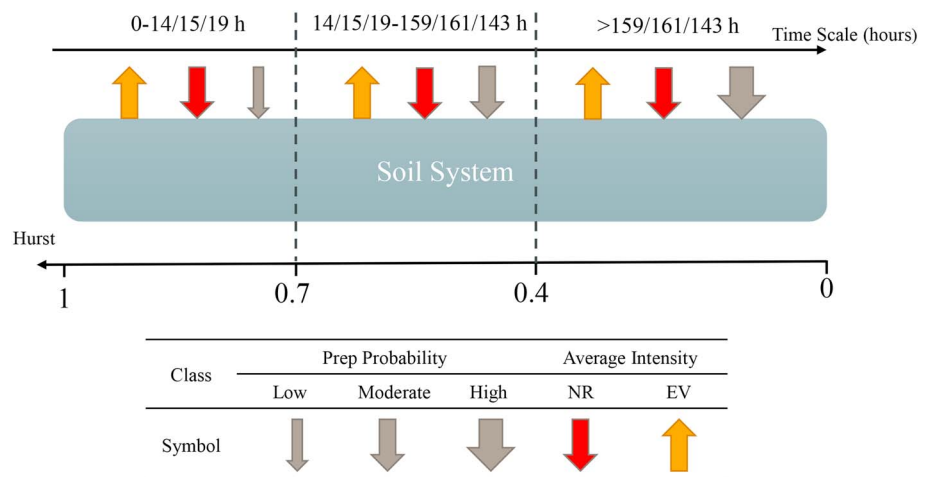


**Figure 7.** Sponge concept diagram of Hurst exponents for soil moisture dynamics where the yellow, red, and gray arrows denote evapotranspiration intensity (EV), net radiation intensity (NR), and precipitation probability (Prep), respectively. The widths of the gray arrows are proportional to the precipitation probability levels. The time scale axis denotes time scale ranges for three depths (4, 10, and 20 cm). The Hurst axis denotes the soil moisture Hurst range of the three depths.

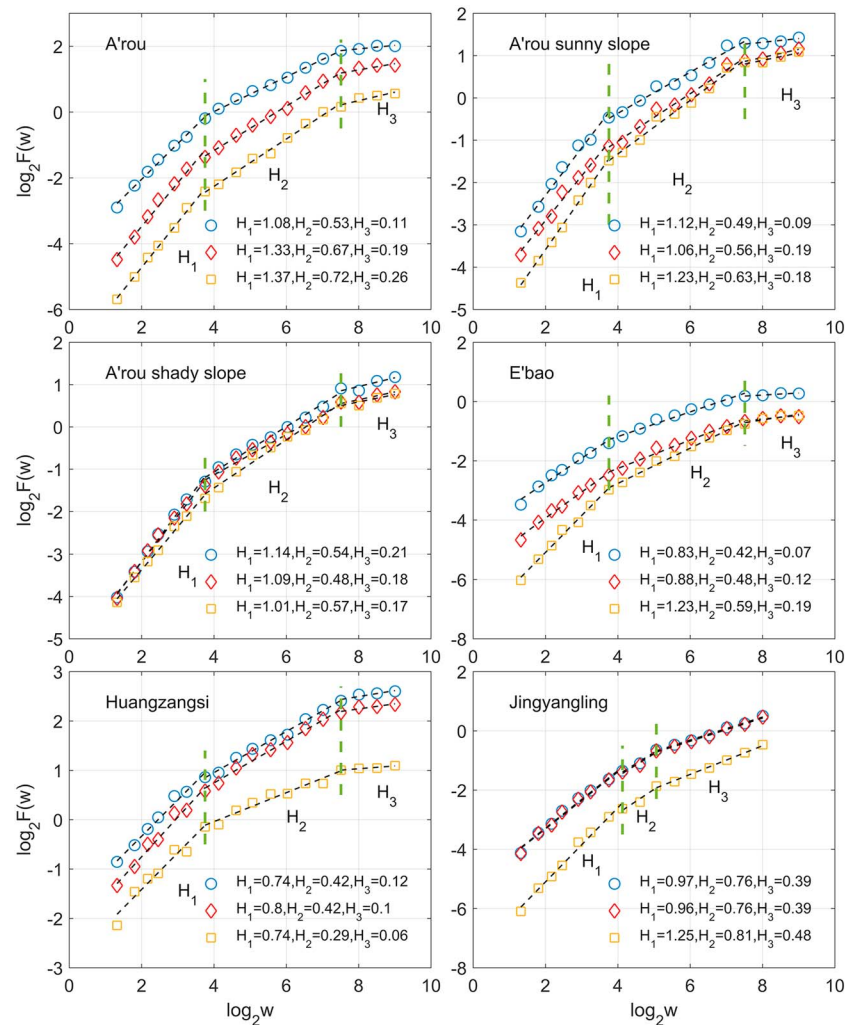


**Figure 8.** Adaptive fractal analysis of soil moisture for 1 June to 31 August 2014, for depths of 4 (blue circles), 10 (red diamonds), and 20 cm (yellow squares) for six automatic monitoring stations.

of soil moisture for the three stations. Figures S28–S30 show CCDF results of precipitation intervals for the three stations. Figures S38–S40 show AFA results of net radiation for the three stations.

Although the three stations are characterized by different land cover and vegetation types (the Shenshawo station is located on desert land), the persistence of soil moisture observed at three depths from these stations reveals the presence of significant multiphase patterns. These results are consistent with those of the above analysis. While vegetation water uptake certainly affects the soil moisture dynamics, it may not impact persistence and corresponding time scales as much as net radiation and precipitation. Moreover, the net radiation also reflects certain aspects of the water uptakes of vegetation because the vegetation is characterized by strong water uptakes with strong radiation due to transpiration effects.

#### 4. Discussion

Based on the above analysis, Hurst exponents depict the conversion of soil moisture dynamics. When Hurst exponents are greater than 0.5 or even 1, soil moisture dynamics present strong long-range correlations and can even become nonstationary over the short time scales. This indicates that soil moisture is more likely to decrease in the future when it has already decreased now and vice versa. When Hurst exponents fluctuate by approximately 0.5 at moderate time scales, soil moisture dynamics show a weak long-range correlation or antipersistence. When the Hurst exponents range between 0 and 0.5 over a long time scale, soil moisture

exhibits antipersistence. This indicates that the soil moisture is more likely to increase in the future when it has already decreased and vice versa.

According to our AFA results of net radiation, soil moisture dynamics exhibit a pattern similar to that observed for net radiation over short time scales (over approximately 14 hr at 4 cm, 15 hr at 10 cm, and 19 hr at 20 cm on average). Simultaneously, the probability of precipitation is low according to the CCDF of precipitation intervals. This proves that soil moisture is mainly influenced by net radiation or precipitation. However, at moderate time scales (over approximately 14 to 159 hr at 4 cm, 15 to 161 hr at 10 cm, and 19 to 143 hr at 20 cm on average), net radiation exhibits antipersistence while the precipitation probability is moderate. Hence, the long-range correlation of soil moisture is weakened or enters antipersistence. Over the long time scale (after 159 hr at 4 cm, after 161 hr at 10 cm, and after 143 hr at 20 cm on average), the probability of precipitation is very high and soil moisture is supplemented with water supplies. Thus, soil moisture dynamics show signs of antipersistence, as soil moisture reverts to a dry condition without disturbances over the long term.

In summary, in an environment such as the BRB, which involves minimal anthropogenic activities, soil moisture dynamics can be illustrated by the three-phase sponge concept diagram shown in Figure 7 due to similar water retention and release patterns observed in soil and sponges (Richardson & Siccama, 2000). The diagram illustrates a scenario in which a sponge is constantly losing water but will recover to a normal state with an additional water supply (e.g., rainfall). At short time scales, either strong net radiation processes or precipitation controls soil moisture dynamics by affecting evapotranspiration and soil water conditions. At moderate time scales, net radiation and moderate precipitation probabilities have a moderate evapotranspiration effect and exhibit moderate soil water supply probability, respectively. Therefore, soil moisture dynamics are likely to change under dry conditions. However, at long time scales, the combination of high water supply probability and average net radiation intensity increases soil water supply probability levels. Consequently, soil moisture dynamics are very likely to shift from dry to wet.

Most of our soil moisture AFA results adhere to this concept diagram. For example, Figure 8 shows six stations at which soil moisture exhibits typical patterns of strong long-range correlation (even nonstationarity) to strong antipersistence. Some special examples can also be explained by this diagram, although they differ from typical cases. For instance, soil moisture dynamics observed at 4 cm for WSNN #35 show long-range correlations at short and moderate time scales because their Hurst exponents are slightly greater than 0.5. This issue is likely attributable to the occurrence of weak evapotranspiration processes, which are influenced by geographic factors (e.g., slope and aspect) at the WSNN #35 station.

## 5. Conclusions

The soil moisture dynamics show different levels of persistence at different scaling ranges based on the AFA results. At a short time scale, soil moisture mostly demonstrates a strong long-range correlation with  $H > 0.7$ . At a moderate time scale, most soil moisture shows a weak long-range correlation or antipersistence with  $0.4 < H < 0.7$ . At a long time scale, soil moisture mostly exhibits strong signs of antipersistence with  $0 < H < 0.4$ . In addition, scaling estimators of Hurst exponents for soil moisture depict effects of net radiation and precipitation. Therefore, Hurst exponents and scaling region estimators can illustrate the persistence of soil moisture dynamics. These parameters can enhance our understanding of soil systems and improve existing simulation models. For example, in situ monitoring data are essential reference materials for remote sensing data. Evolution laws and temporal rhythm of soil moisture investigated from in situ monitoring data are critical for the downscaling of remote sensing data. Persistence and time scales can be used to determine the proper time scale for downscaling soil moisture remote sensing data. Meanwhile, according to radiation time scale, we can determine how long soil moisture is likely to decrease to enhance the effectiveness of radiation for the model. In addition, based on rainfall conditions and the persistence of soil moisture, the climate model can reconsider how soil moisture develops at different time scales.

However, the results of the AFA also show that shallow soil moisture dynamics change slightly at different depths, possibly because this study focused on shallow soil layers of soil moisture dynamics, which are rarely influenced by deeper hydrological processes (e.g., groundwater table). Therefore, soil moisture dynamics observed in deeper soil layers and other environments should be investigated and analyzed in future works. Additionally, due to the lack of long-term fine monitoring data, the estimated time scales and Hurst exponents must be further explored for different climatic zones and geographic environment. The relationship

between the scaling range estimators of Hurst exponents and precipitation intervals should also be further investigated using more sample stations.

#### Acknowledgments

We would like to thank the anonymous reviewers for their constructive comments and suggestions on the manuscript. This work was supported by National Key R&D Program of China (2017YFA0604704), National Natural Science Foundation of China (91725000), and the Fundamental Research Funds for the Central Universities. The data used in this study are available from Environmental and Ecological Science Data Center for West China at <http://www.heihedata.org/>.

#### References

- Bosch, D. D., Lakshmi, V., Jackson, T. J., Choi, M., & Jacobs, J. M. (2006). Large scale measurements of soil moisture for validation of remotely sensed data: Georgia soil moisture experiment of 2003. *Journal of Hydrology*, 323(1), 120–137. <https://doi.org/10.1016/j.jhydrol.2005.08.024>
- Brocca, L., Melone, F., Moramarco, T., & Wagner, W. (2010). Improving runoff prediction through the assimilation of the ASCAT soil moisture product. *Hydrology and Earth System Sciences Discussions*, 14(10), 1881–1893. <https://doi.org/10.5194/hessd-7-4113-2010>
- Brocca, L., Tullio, T., Melone, F., Moramarco, T., & Morbidelli, R. (2012). Catchment scale soil moisture spatial-temporal variability. *Journal of Hydrology*, 422–(423), 63–75. <https://doi.org/10.1016/j.jhydrol.2011.12.039>
- Bunde, A., & Havlin, S. (2002). Power-law persistence in the atmosphere and in the oceans. *Physica A: Statistical mechanics and its applications*, 314(1–4), 15–24. [https://doi.org/10.1016/S0378-4371\(02\)01050-6](https://doi.org/10.1016/S0378-4371(02)01050-6)
- Bunde, A., Havlin, S., Koscielny-Bunde, E., & Schellnhuber, H.-J. (2001). Long term persistence in the atmosphere: Global laws and tests of climate models. *Physica A: Statistical Mechanics and Its Applications*, 302(1–4), 255–267. [https://doi.org/10.1016/S0378-4371\(01\)00469-1](https://doi.org/10.1016/S0378-4371(01)00469-1)
- Cho, E., & Choi, M. (2014). Regional scale spatio-temporal variability of soil moisture and its relationship with meteorological factors over the Korean peninsula. *Journal of Hydrology*, 516, 317–329. <https://doi.org/10.1016/j.jhydrol.2013.12.053>
- Daly, E., & Porporato, A. (2005). A review of soil moisture dynamics: From rainfall infiltration to ecosystem response. *Environmental Engineering Science*, 22(1), 9–24. <https://doi.org/10.1089/ees.2005.22.9>
- Famiglietti, J. S., Devereaux, J. A., Laymon, C. A., Tsegaye, T., Houser, P. R., Jackson, T. J., & van Oevelen, P. J. (1999). Ground-based investigation of soil moisture variability within remote sensing footprints during the Southern Great Plains 1997 (SGP97) hydrology experiment. *Water Resources Research*, 35(6), 1839–1851. <https://doi.org/10.1029/1999WR900047>
- Fitzjohn, C., Ternan, J. L., & Williams, A. G. (1998). Soil moisture variability in a semi-arid gully catchment: Implications for runoff and erosion control. *Catena*, 32(1), 55–70. [https://doi.org/10.1016/S0341-8162\(97\)00045-3](https://doi.org/10.1016/S0341-8162(97)00045-3)
- Gao, J., Cao, Y., Tung, W., & Hu, J. (2007). *Multiscale analysis of complex time series: Integration of chaos and random fractal theory, and beyond*. Hoboken, NJ: John Wiley.
- Gao, J., Fang, P., & Liu, F. (2017). Empirical scaling law connecting persistence and severity of global terrorism. *Physica A: Statistical Mechanics and Its Applications*, 482(Supplement C), 74–86. <https://doi.org/10.1016/j.physa.2017.04.032>
- Gao, J., Gurbaxani, B., Hu, J., Heilman, K., Emauele, V., Lewis, G., & Lin, J.-M. (2013). Multiscale analysis of heart rate variability in non-stationary environments. *Frontiers in Physiology*, 4, 119. <https://doi.org/10.3389/fphys.2013.00119>
- Gao, J., Hu, J., Mao, X., & Perc, M. (2012). Culturomics meets random fractal theory: Insights into long-range correlations of social and natural phenomena over the past two centuries. *Journal of The Royal Society Interface*, 9(73), 1956–1964. <https://doi.org/10.1098/rsif.2011.0846>
- Gao, J., Hu, J., & Tung, W. (2011). Facilitating joint chaos and fractal analysis of biosignals through nonlinear adaptive filtering. *PLoS ONE*, 6(9), 1–8. <https://doi.org/10.1371/journal.pone.0024331>
- Gao, J., Hu, J., Tung, W.-W., Cao, Y., Sarshar, N., & Roychowdhury, V. P. (2006). Assessment of long-range correlation in time series: How to avoid pitfalls. *Physical Review E*, 73(1), 16117.
- Gao, X., Liu, Y., Guo, J., & Wang, Y. (2015). Application of R/S method to dynamic analysis of soil moisture content in Luancheng District of Shijiazhuang City. *Journal of Hohai University (Natural Sciences)*, 43(1), 72–77. <https://doi.org/10.3876/j.issn.1000-1980.2015.01.014>
- Ge, Y., Wang, J. H., Heuvelink, G. B. M., Jin, R., & Li, X. (2015). Sampling design optimization of a wireless sensor network for monitoring ecohydrological processes in the Babao River Basin, China. *International Journal of Geographical Information Science*, 29(1), 92–110. <https://doi.org/10.1080/13658816.2014.948446>
- Gebremichael, M., Rigon, R., Bertoldi, G., & Over, T. M. (2009). On the scaling characteristics of observed and simulated spatial soil moisture fields. *Nonlinear Processes in Geophysics*, 16(1), 141–150. <https://doi.org/10.5194/npg-16-141-2009>
- Ghannam, K., Nakai, T., Paschalis, A., Oishi, C. A., Kotani, A., Igarashi, Y., & Katul, G. G. (2016). Persistence and memory timescales in root-zone soil moisture dynamics. *Water Resources Research*, 52, 1427–1445. <https://doi.org/10.1002/2015WR017983>
- Guerrini, I., & Swartzendruber, D. (1997). Fractal concepts in relation to soil water diffusivity. *Soil Science*, 162(11), 778–784.
- Hirschi, M., Seneviratne, S. I., Alexandrov, V., Boberg, F., Boroneant, C., Christensen, O. B., & Stepanek, P. (2010). Observational evidence for soil-moisture impact on hot extremes in southeastern Europe. *Nature Geoscience*, 4, 17. <https://doi.org/10.1038/ngeo1032>
- Hu, J., Gao, J., & Wang, X. (2009). Multifractal analysis of sunspot time series: The effects of the 11-year cycle and Fourier truncation. *Journal of Statistical Mechanics: Theory and Experiment*, 2009(2), P02066. <http://stacks.iop.org/1742-5468/2009/i=02/a=P02066>
- Hurst, H. E. (1951). Long term storage capacities of reservoirs. *Transactions of the American Society of Civil Engineers*, 116(12), 776–808.
- Janatian, N., Sadeghi, M., Sanaeinejad, S. H., Bakhshian, E., Farid, A., Hasheminia, S. M., & Ghazanfari, S. (2017). A statistical framework for estimating air temperature using MODIS land surface temperature data. *International Journal of Climatology*, 37(3), 1181–1194. <https://doi.org/10.1002/joc.4766>
- Ji, W., Lin, M., Biswas, A., Si, B. C., Chau, H. W., & Cresswell, H. P. (2016). Fractal behavior of soil water storage at multiple depths. *Nonlinear Processes in Geophysics*, 23(4), 269–284. <https://doi.org/10.5194/npg-23-269-2016>
- Jiang, A., & Gao, J. (2016). Fractal analysis of complex power load variations through adaptive multiscale filtering. In *Economic and Socio-cultural Computing (BESC) in International Conference on Behavioral* (pp. 1–5). <https://doi.org/10.1109/BESC.2016.7804502>
- Koster, R. D., Mahanama, S. P. P., Livneh, B., Lettenmaier, D. P., & Reichle, R. H. (2010). Skill in streamflow forecasts derived from large-scale estimates of soil moisture and snow. *Nature Geoscience*, 3(9), 613–616. <https://doi.org/10.1038/ngeo944>
- Koster, R. D., & Suarez, M. J. (2003). Impact of land surface initialization on seasonal precipitation and temperature prediction. *Journal of Hydrometeorology*, 4(2), 408–423.
- Kurc, S. A., & Small, E. E. (2007). Soil moisture variations and ecosystem-scale fluxes of water and carbon in semiarid grassland and shrubland. *Water Resources Research*, 43, W06416. <https://doi.org/10.1029/2006WR005011>
- Li, X., Cheng, G., Liu, S., Xiao, Q., Ma, M., Jin, R., & Xu, Z. (2013). Heihe watershed allied telemetry experimental research (hi WATER): Scientific objectives and experimental design. *Bulletin of the American Meteorological Society*, 94(8), 1145–C1160. <https://doi.org/10.1175/BAMS-D-12-00154.1>
- Liu, Z., Wang, L., Yu, X., Wang, S., Deng, C., Xu, J., & Bai, L. (2017). Multi-scale response of runoff to climate fluctuation in the headwater region of the Kaidu River in Xinjiang of China. *Atmospheric Science Letters*, 18(5), 230–236. <https://doi.org/10.1002/asl.747>
- Liu, S., Xu, Z., Wang, W. Z., Jia, Z. Z., Zhu, M. J., Bai, J., & Wang, J. (2011). A comparison of eddy-covariance and large aperture scintillometer measurements with respect to the energy balance closure problem. *Hydrology and Earth System Sciences*, 15(4), 1291–1306. <http://www.hydrol-earth-syst-sci.net/15/1291/>

- Luo, K., Tao, F., Deng, X., & Moiwu, J. P. (2017). Changes in potential evapotranspiration and surface runoff in 1981–2010 and the driving factors in upper Heihe River basin in northwest China. *Hydrological Processes*, 31(1), 90–103. <https://doi.org/10.1002/hyp.10974>
- Mei, R., & Wang, G. (2011). Impact of sea surface temperature and soil moisture on summer precipitation in the United States based on observational data. *Journal of Hydrometeorology*, 12(5), 1086–1099.
- Millán, H., Cumbreira, R., & Tarquis, A. M. (2016). Multifractal and Levy-stable statistics of soil surface moisture distribution derived from 2D image analysis. *Applied Mathematical Modelling*, 40(3), 2384–2395. <https://doi.org/10.1016/j.apm.2015.09.063>
- Mirás-Avalos, J. M., Trigo-Clórdoba E., Silva-Dias, D., Varela-Vila, R. I., & García-Tomillo, A. (2016). Multifractal behaviour of the soil water content of a vineyard in northwest Spain during two growing seasons. *Nonlinear Processes Geophysics*, 23(4), 205–213. <https://doi.org/10.5194/npg-23-205-2016>
- Orth, R., & Seneviratne, S. I. (2012). Analysis of soil moisture memory from observations in Europe. *Journal of Geophysical Research*, 117, D15115. <https://doi.org/10.1029/2011JD017366>
- Peng, C. K., Buldyrev, S., Havlin, S., Simons, M., Stanley, H. E., & Goldberger, A. L. (1994). Mosaic organization of DNA nucleotides. *Physical Review E*, 49(2), 1685–1689. <https://doi.org/10.1103/PhysRevE.49.1685>
- Richardson, A. D., & Siccama, T. G. (2000). Are soils like sponges? *JAWRA Journal of the American Water Resources Association*, 36(4), 913–918. <https://doi.org/10.1111/j.1752-1688.2000.tb04316.x>
- Schertzer, D., Tchiguirinskaia, I., Lovejoy, S., & Hubert, P. (2010). No monsters, no miracles: In nonlinear sciences hydrology is not an outlier!. *Hydrological Sciences Journal*, 55(6), 965–979. <https://doi.org/10.1080/02626667.2010.505173>
- Seneviratne, S. I., Corti, T., Davin, E. L., Hirschi, M., Jaeger, E. B., Lehner, I., & Teuling, A. J. (2010). Investigating soil moisture–climate interactions in a changing climate: A review. *Earth-Science Reviews*, 99(3), 125–161. <https://doi.org/10.1016/j.earscirev.2010.02.004>
- Sengupta, S., Biswas, S., Nag, S., Sanyal, S., Banerjee, A., Sengupta, R., & Ghosh, D. (2017). Emotion specification from musical stimuli: An EEG study with AFA and DFA. In *2017 4th International Conference on Signal Processing and Integrated Networks (SPIN)* (pp. 596–600). <https://doi.org/10.1109/SPIN.2017.8050019>
- Song, R., Yu, J., & Liu, C. (2011). Long-range correlations of soil moisture series with detrended fluctuation analysis. *Journal of Hydraulic Engineering*, 42(3), 315–322.
- Song, C., Yuan, L., Yang, X., & Fu, B. (2017). Ecological-hydrological processes in arid environment: Past, present and future. *Journal of Geographical Sciences: Atmospheres*, 27, 1577–1594. <https://doi.org/10.1007/s11442-017-1453-x>
- Sun, S., & Wang, G. (2012). The complexity of using a feedback parameter to quantify the soil moisture-precipitation relationship. *Journal of Geophysical Research*, 117, D11113. <https://doi.org/10.1029/2011JD017173>
- Tian, J., Zhang, B., He, C., & Yang, L. (2017). Variability in soil hydraulic conductivity and soil hydrological response under different land covers in the mountainous area of the Heihe River watershed, northwest China. *Land Degradation and Development*, 28(4), 1437–1449. <https://doi.org/10.1002/ldr.2665>
- Tuttle, S., & Salvucci, G. (2016). Empirical evidence of contrasting soil moisture-precipitation feedbacks across the United States. *Science*, 352(6287), 825–828. <https://doi.org/10.1126/science.aaa7185>
- Vereecken, H., Huisman, J. A., Pachepsky, Y., Montzka, C., van der Kruk, J., Bogaen, H., & Vanderborght, J. (2014). On the spatio-temporal dynamics of soil moisture at the field scale. *Journal of Hydrology*, 516(Supplement C), 76–96. <https://doi.org/10.1016/j.jhydrol.2013.11.061>
- Vidal-Vazquez, E., Paz-Ferreiro, J., Vieira, S., Topp, G., Miranda, J., & Paz Gonzalez, A. (2012). Fractal description of the spatial and temporal variability of soil water content across an agricultural field. *Soil Science*, 177(2), 131–138. <https://doi.org/10.1097/SS.0b013e318241119a>
- Zhao, X., Chen, X., & Huang, Q. (2017). Trend and long-range correlation characteristics analysis of runoff in upper Fenhe River basin. *Water Research*, 44(1), 31–42. <https://doi.org/10.1134/S0097807817010201>
- Zhu, H. B., & Gao, J. B. (2014). Fractal behavior in the headway fluctuation simulated by the Nasch model. *Physica A: Statistical Mechanics and Its Applications*, 398, 187–193. <https://doi.org/https://doi.org/10.1016/j.physa.2013.12.033>